Nanoparticle core size optimization for magnetic particle imaging

Carolyn Shasha[1], Eric Teeman[2], and Kannan M. Krishnan[1,2]

[1] *Department of Physics, University of Washington, Seattle, USA*
[2] *Department of Materials Sciences & Engineering, University of Washington, Seattle, USA*

July 30, 2019

Abstract In magnetic particle imaging (MPI), the changing magnetization of magnetic nanoparticle (MNP) tracers subjected to an alternating magnetic field is detected. The physical properties of the MNP tracers have a direct effect on the quality of the resulting signal. In order to improve MPI image resolution and sensitivity, optimizing these properties, in particular the MNP core size, is essential. In this work, we investigate the existence of an optimal MNP core size for MPI using stochastic simulations of Langevin equations, supported by magnetic particle spectroscopy (MPS) measurements of highly monodisperse single-core nanoparticles with carefully tailored core sizes. We demonstrate that once the MNP core diameter exceeds around 28 nm (with the exact value depending on applied field properties and non-magnetic nanoparticle coating), relaxation effects will begin to dominate. Furthermore, as nanoparticle size is increased, interparticle interactions make it difficult to stabilize the particles in water and maintain their monodispersity. Taken together, we conclude that 28 nm in core diameter is an optimal size for single-core, monodisperse, magnetite particles used in MPI.

1 Introduction

Since MPI was initially proposed in 2006 [1], there has been significant progress in improving MPI image quality, with hardware, software, and tracer development [2]. However, in order for MPI to become a fully viable and competitive medical imaging platform, for example when compared with magnetic resonance imaging (MRI) or computed tomography (CT), further progress in improving spatial resolution and image sensitivity is required. In particular, while developments in tracer fabrication technology have enabled fabrication of monodisperse spherical single-phase magnetite nanoparticles which result in significant improvement to MPI image quality [3, 4, 5, 6, 7], opportunities for optimization of the magnetic properties of MNP tracers remain.

The spatial resolution of a given MPI image is dependent on hardware parameters, such as the gradient field strength. The resolution will be directly (inversely) proportional to the gradient field; current scanners use a gradient field of 1-7 $(\mathrm{T/m})/\mu_0$ [8], but hardware limits impose difficulties in increasing the gradient field strength indefinitely. Increasing the saturation magnetization of iron oxide MNPs by controlling their oxidation state, and tailoring their shape, crystallinity, and monodispersity, also improves MPI signal strength and image resolution [9]. Optimization of these tracer properties for improved MPI performance, both from a theoretical and experimental perspective, has been the subject of substantial investigation: for example, optimizing oxidation state and crystallinity to improve saturation magnetization was studied in Refs. [4, 10]; the effect of changing anisotropy on magnetic performance was examined in Refs. [11, 12]; and the effect of size distribution was studied in Refs. [13, 14]. It is well known that nanoparticle size, particularly the magnetic core size, has a significant effect on the resulting MPI signal. It is commonly believed that there is an optimal size for MPI as a result of relaxation effects that arise at large sizes, which has been indicated by experiment. Optimization of nanoparticle size for MPI has been investigated experimentally in Refs. [5, 15, 16, 3] and theoretically in [17, 18, 11, 19]. However, there are limitations to these prior studies; the theoretical simulation-based studies that have been performed to predict optimal core size rely on overly simplistic models of nanoparticle dynamics, such as the Langevin model or Debye linear response theory, which cannot accurately describe the nonlinear behavior that arises under the fields applied in MPI [20]. Furthermore, applied field conditions and surface functionalization is often ignored, despite the fact that these factors can significantly affect the optimal size that should be used. While more advanced models and simulation techniques have been developed and applied to MPI, they have not yet been used to study core size optimization specifically [21, 22, 23]. This will be the goal of the present work, as well as quantitatively incorporating effects beyond relaxation, namely agglomeration, in the investigation of optimal size for MPI.

The point-spread function (PSF), defined as the derivative of the particle magnetization with respect to the applied field, can be used to estimate the resulting signal strength and image resolution of an MPI image generated from a particular MNP tracer. The height of the PSF peak will determine the sensitivity and indicate the signal-to-noise ratio (SNR) of the resulting image. The image resolution is defined by the minimum distance that two samples can be separated by while remaining separately distinguishable. This requires a significant minimum in signal between the two samples, where the minimum value must be less than half of the maximum value at the sample positions. From that definition, the estimated image resolution from a given MNP sample can be extracted from the full-width-at-half-maximum (FWHM) of the PSF. The FWHM will be indicated here in mT/μ_0, but this measurement can be easily converted to a spatial value by dividing by the strength of the gradient field used in the MPI scanner. For example, a FWHM of 1 mT/μ_0 would correspond to a spatial resolution of 1 mm for a 1 $(\mathrm{T/m})/\mu_0$ gradient field.

If the MNP magnetization is assumed to follow the Langevin function, the magnetization is $M(\xi) = n(\coth\xi - 1/\xi)$, where $\xi = \mu_0 M_s V_c H/k_B T$ and n is the particle concentration, and the PSF will be represented by the derivative of the Langevin function with respect to the applied field. The MNP has saturation magnetization M_s and core volume V_c. H is the applied field in T/μ_0, where μ_0 is the permeability of free space, T is the temperature, and k_B is Boltzmann's constant. In this model, the peak of the PSF will be the value of the derivative of the magnetization when the magnetic field is equal to zero:

$$M'(0) = \frac{n\mu_0(M_s V_c)^2}{3k_B T}. \tag{1}$$

The corresponding FWHM of the PSF peak is approximately [8]:

$$\Delta x_{\mathrm{Langevin}} = \frac{4.16 k_B T}{\mu_0 M_s V_c}. \tag{2}$$

According to this model, then, the signal strength should improve as the square of the core volume, and the resolution is inversely proportional to the volume, implying that core size should be maximized for best image quality. However, as particle core size is increased, relaxation behavior will become more pronounced [2, 3], resulting in reduced signal. Furthermore, in practice, as particle core size is increased, dispersing the MNPs in water and maintaining their monodispersity becomes significantly more difficult due to increased strength of interparticle magnetostatic interactions. It is desirable, then, to identify an optimal size above which relaxation effects are dominant.

When particle relaxation is taken into account (here we assume that all particles have the same effective relaxation time), the PSF can be expressed by a convolution of the adiabatic signal, which we take to be the derivative of the Langevin function, and a relaxation term [8]:

$$\hat{\rho}(x_s(t)) = \hat{\rho}_{\mathrm{Langevin}}(x_s(t)) * \left(\frac{1}{v_s\tau}\right) \exp\left(-\frac{x_s(t)}{v_s\tau}\right) u(x_s), \tag{3}$$

where x_s is the location of the field-free point, τ is the nanoparticle relaxation time, u is the Heaviside step function, and v_s is the velocity of the field-free point of the scanner, equal to $2\pi f_0 H_0/G$, where f_0 and H_0 are the respective frequency and amplitude of the applied field, and G is the strength of the gradient field. Following Ref. [8], we can approximate the total FWHM as a sum of the adiabatic FWHM $\Delta x_{\mathrm{Langevin}}$ and the blur from relaxation $\Delta x_{\mathrm{relax}}$:

$$\Delta x \approx \alpha \Delta x_{\mathrm{Langevin}} + \beta \Delta x_{\mathrm{relax}}. \tag{4}$$

The values for α and β can be experimentally determined from least-squares fitting, and in Ref. [8] were found to be on the order of 1. The FWHM of an exponential decay function $f(t) = \exp(-t/\tau)$ is $\tau\ln(2)$, and so we have:

$$\Delta x_{\mathrm{relax}}(H_0, f_0) = \ln(2) v_s \tau(H_0, f_0). \tag{5}$$

The dependence of Δx on core size is now not trivial, since $\Delta x_{\mathrm{Langevin}}$ decreases with core size while $\Delta x_{\mathrm{relax}}$ scales as the particle relaxation time, which will be a complex function of both particle core and hydrodynamic size (as well as applied field amplitude and frequency). In the following work, we will examine the effects of size-dependent relaxation behavior on the PSF, and use the results to investigate the existence of an optimal MNP core size for MPI image quality.

2 Materials and Methods

2.1 MNP synthesis and preparation

Magnetite nanoparticles were synthesized following a thermal decomposition process, as described in detail in Ref. [4]. Three particle samples were fabricated, with core diameters of 21.9 nm, 25.3 nm, and 27.7 nm, with respective size distribution parameters of 0.04, 0.06, and 0.07, assuming a log-normal distribution of core sizes. All three samples were relatively spherical, with respective average circularity values of 0.878±0.027, 0.890±0.058, and 0.805±0.033. Core sizes and circularity values were determined from transmission electron microscopy (TEM) images using ImageJ software. The nanoparticle cores were coated with approximately 5% loading of 20 kDa poly(ethylene glycol) PEG-based amphiphilic polymer and then dispersed in distilled water at a concentration of 0.9 mgFe/mL, resulting in respective hydrodynamic sizes of 94.5 nm, 77.1 nm, and 95.9 nm, with respective size distribution parameters of 0.13, 0.18, and 0.15, as determined by dynamic light scattering (DLS).

2.2 Magnetic particle spectroscopy

Magnetic particle spectroscopy (MPS) measurements were performed using a home-built spectrometer as described in Ref. [5], with a drive frequency of 26 kHz and upper frequency of 1.05 MHz. 150 μL aqueous solutions of each particle sample were measured by first acquiring a background measurement, inserting the sample to be measured, and taking an average over 10 periods after background subtraction. Three such measurements were performed for each sample, and the results were subsequently averaged, such that the final measurement consists of an average over 30 periods of the drive field.

2.3 Landau-Lifshitz-Gilbert simulations

Stochastic simulations of coupled Langevin equations were performed according to Refs. [24, 20]. In brief, the direction of the internal particle magnetization, $\mathbf{m}$, and the direction of the easy axis, $\mathbf{n}$, will rotate according to:

$$\frac{\mathrm{d}\mathbf{m}}{\mathrm{d}t} = \frac{\gamma}{1+\alpha^2}(\mathbf{H} + \alpha\mathbf{m}\times\mathbf{H})\times\mathbf{m} \tag{6}$$

$$\frac{\mathrm{d}\mathbf{n}}{\mathrm{d}t} = \frac{\mathbf{\Theta}}{6\eta V_\mathrm{h}}\times\mathbf{n}, \tag{7}$$

where γ is the electron gyromagnetic ratio, α is the dimensionless damping coefficient, and η is the viscosity of the surrounding medium. $\mathbf{H}$ and Θ are the respective effective magnetic field and torque acting on the particle. The particle energy, excluding interparticle interactions, is:

$$U = -\mu_0 M_s V_c \mathbf{m}\cdot\mathbf{H}_\mathrm{app} - KV_\mathrm{c}(\mathbf{m}\cdot\mathbf{n})^2, \tag{8}$$

where the applied field is represented by $\mathbf{H}_\mathrm{app}$, and K is the effective particle anisotropy. To find the effective field and torque, we take derivatives of the energy and add thermal fluctuations:

$$\mathbf{H} = -\frac{1}{\mu_0 M_s V_c}\frac{\partial U}{\partial \mathbf{m}} + \mathbf{H}_\mathrm{th} \tag{9}$$

$$\Theta = \frac{\partial U}{\partial \mathbf{n}}\times\mathbf{n} + \Theta_\mathrm{th}. \tag{10}$$

We assume that $\mathbf{H}_\mathrm{th}$ and Θ_th are Gaussian stochastic processes, with a mean of zero and correlations:

$$\left\langle \mathbf{H}^i_\mathrm{th}(t)\mathbf{H}^j_\mathrm{th}(t')\right\rangle = \frac{2k_BT}{\gamma M_s V_c}\frac{1+\alpha^2}{\alpha}\delta_{ij}\delta(t-t') \tag{11}$$

$$\left\langle \Theta^i_\mathrm{th}(t)\Theta^j_\mathrm{th}(t')\right\rangle = 12k_BT\eta V_\mathrm{h}\delta_{ij}\delta(t-t'). \tag{12}$$

The equations are integrated according to the Stratanovich-Heun method. Simulations were performed with 10 000 time steps per field cycle, resulting in time steps on the order of nanoseconds for field frequencies in the tens of kilohertz range. For each simulation, 60 000 particles were simulated at a time, and the magnetization was then averaged. K was initially set to 5 kJ/m^3 and M_s was set to 420 kA/m for all simulations. For comparison, simulations were repeated for K values up to 11 kJ/m^3. A log-normal size distribution was assumed for all

simulations, with size distribution parameter $\sigma = 0.1$. The value for the anisotropy constant, K, was chosen based on previous work in which the effective anisotropy constant was measured using several characterization methods [25], and verified by fitting to measured MPS data. The effect of changing the anisotropy constant in the context of size optimization was studied previously to that in an earlier work [11]; however, in that work, a much more simplistic theoretical model was employed.

3 Results

The PSF peak height and FWHM were extracted from MPS measurements at three different field amplitudes, with results shown in Fig. 1. As is consistent with past results [5], the predicted image resolution worsens with increasing field amplitude. For all three amplitudes, there is a general decrease in FWHM with core size, and a general increase in signal strength. However, while increasing the core size from 21.9 nm to 25.3 nm results in significant improvement both in terms of signal strength and resolution, a much smaller improvement is seen when further increasing the size from 25.3 nm to 27.7 nm. These results are in sharp contrast to those predicted by the Langevin model (i.e. Eqs. 1 and 2), which predicts that the FWHM should decrease as the cube of the particle diameter, and that the peak should increase as the sixth power of the diameter. The results here indicate that further increasing the size past 28 nm may not have a significant impact on the signal; possible reasons for this are explored using simulations.

PSFs were simulated for a range of particle sizes and applied fields. Results with a fixed frequency of 25 kHz and hydrodynamic diameter of 50 nm are shown in Fig. 2. The trends are consistent with those seen in the MPS data; past a certain core size (e.g. ∼30 nm for an amplitude of 35 mT/μ_0), there is minimal improvement to the resolution, as indicated by the fact that the FWHM appears to asymptote at large core sizes. While the PSF peak continually increases with core size, the rate of increase slows past ∼30 nm.

To understand the effects of each term in Eq. 4, simulations were run under identical conditions but with a larger hydrodynamic size of 150 nm, which should have the effect of inhibiting the nanoparticles Brownian rotational component (the physical rotation of the nanoparticle), so that Néel relaxation dominates, effectively increasing the total relaxation time. Results are shown in Fig. 3. In this case, it can be clearly seen that relaxation behavior dominates above around 30 nm, ultimately decreasing the signal quality. Missing values in Fig. 3 (e.g. FWHM values above 31 nm for a 15 mT/μ_0 field) are due to the extreme phase lag between the applied field and the nanoparticle response, which results in inaccurate FWHM values when the particle's magnetization does not saturate before the field is switched. For that reason, those values were removed.

In order to verify the underlying physical behavior, the effective relaxation time can be extracted from the phase lag ϕ in the simulation data, as $\tan\phi = 2\pi f_0 \tau$. The effective relaxation time for both hydrodynamic diameters is shown in Fig. 4, which confirms that for particles with core size greater than ∼23 nm, the relaxation time is higher for the larger hydrodynamic size. In this case, the relaxation term in Eq. 4 dominates, resulting in an eventual predicted decrease in image quality with increasing size.

4 Discussion

The results indicate that there is a certain core size, which we will label d_c', above which relaxation effects will dominate, and improvements to the MPI signal will slow significantly and potentially reverse. As a first approximation, we hypothesize that this transition occurs when both terms in Eq. 4 are approximately equal, i.e. when $\alpha\Delta x_{\text{Langevin}} \approx \beta\Delta x_{\text{relax}}$. Since α and β are both on the order of 1, we will further assume $\alpha \approx \beta \approx 1$. At a particular value of the effective relaxation time, τ', $\Delta x_{\text{Langevin}} = \Delta x_{\text{relax}}$:

$$\ln(2) v_s \tau' = \frac{4.16 k_B T}{\mu_0 M_s V_c} \tag{13}$$

Solving for τ' then gives us:

$$\tau' = \frac{4.16 k_B T}{\ln(2) v_s \mu_0 M_s V_c} \tag{14}$$

We propose that when $\tau > \tau'$, relaxation behavior will dominate and improvements to the MPI image signal will be minimal. The effective relaxation time can be extracted from the stochastic simulations, which we will explicitly label τ_{ss} for clarity. By plotting τ_{ss} and τ' as a function of core size (see Fig. 5), we can extract the core size d_c' at which $\tau_{ss} = \tau'$.

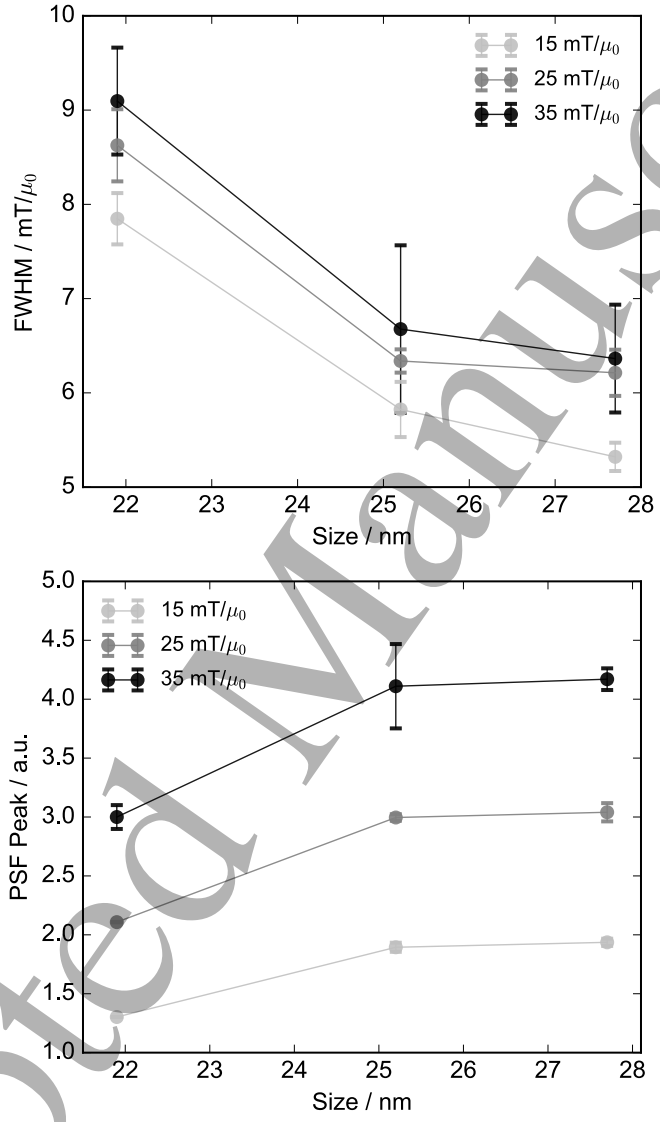

Figure 1: FWHM (top) and peak height (bottom) as a function of core size extracted from MPS data for three different applied field amplitudes, indicating overall signal improvement with core size. The error bars indicate the variance between the forward (increasing field) and reverse (decreasing field) traces.

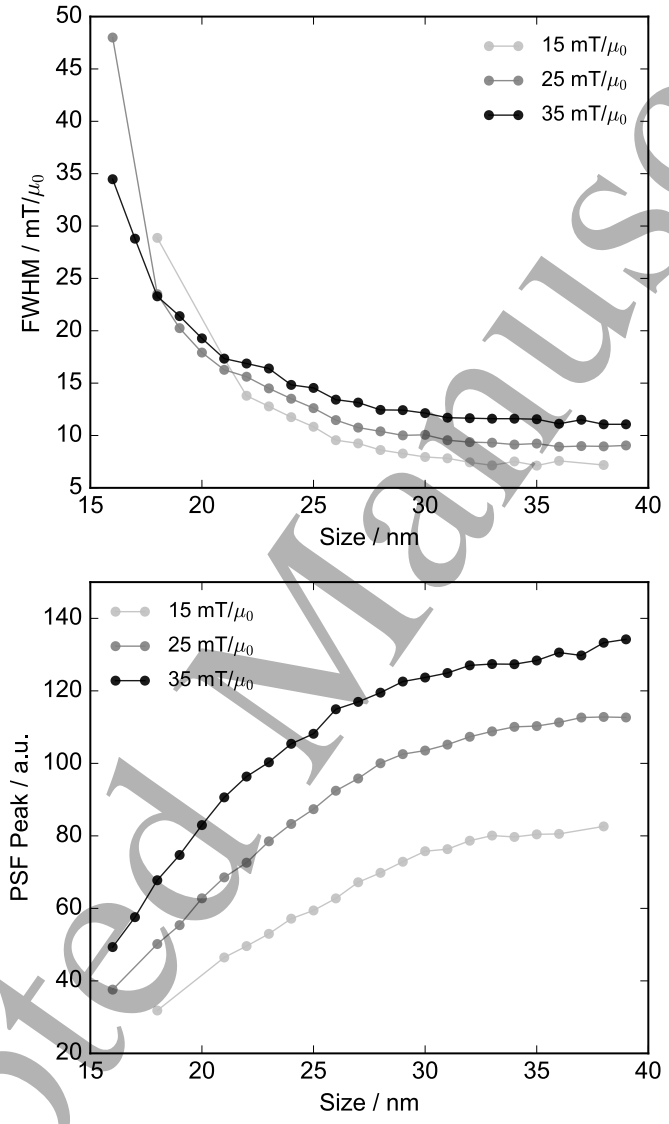

Figure 2: FWHM (top) and peak height (bottom) as a function of core size extracted from stochastic simulations for three different applied field amplitudes and a 50 nm hydrodynamic size, with an applied frequency of 25 kHz. The FWHM appears to asymptote at large core sizes.

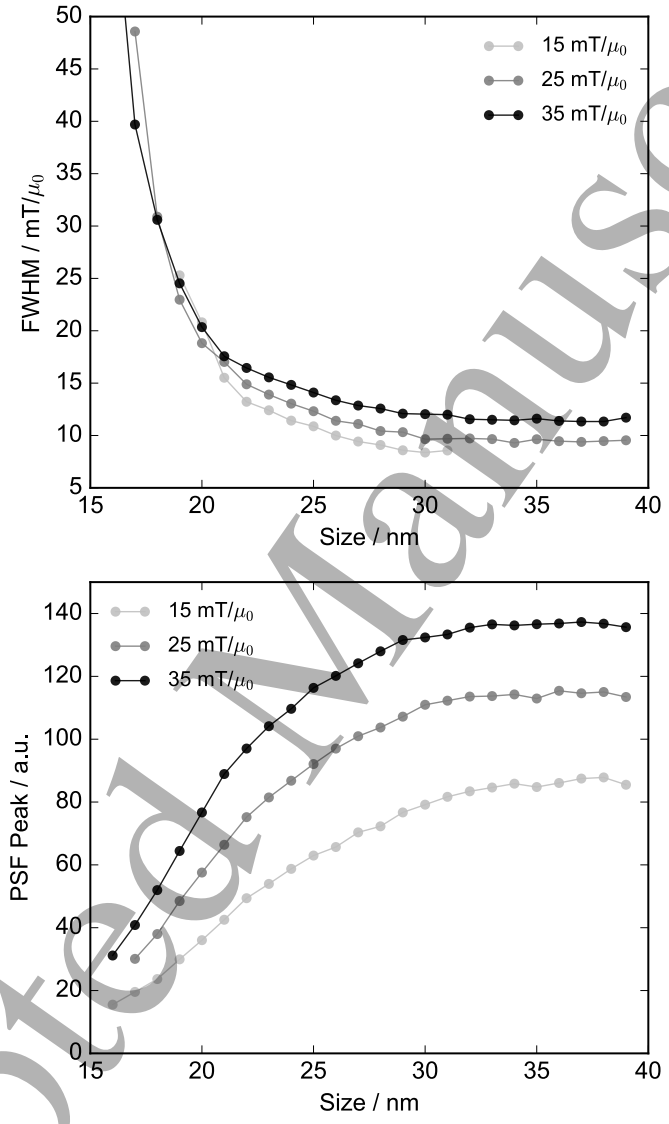

Figure 3: FWHM (top) and peak height (bottom) as a function of core size extracted from stochastic simulations for three different applied field amplitudes and a 150 nm hydrodynamic size, with an applied frequency of 25 kHz. The FWHM appears to asymptote at large core sizes.

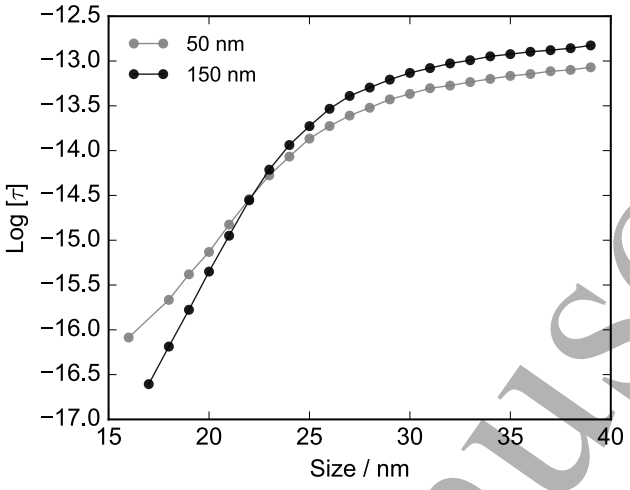

Figure 4: Effective relaxation time extracted from simulations for particles with two different hydrodynamic diameters under an applied field with frequency 25 kHz and amplitude 25 mT/μ_0.

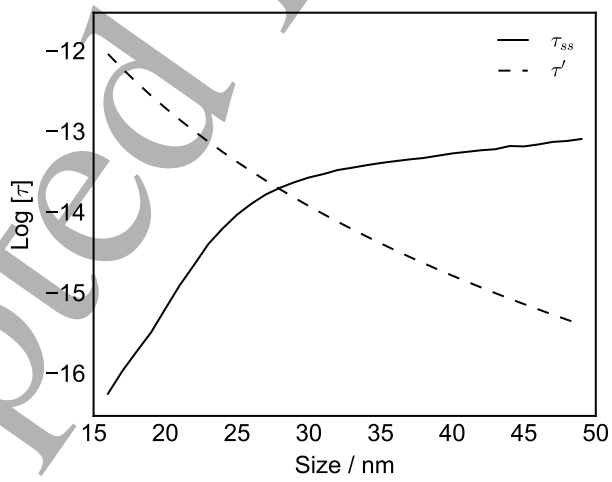

Figure 5: Relaxation time (solid) extracted from stochastic simulations with a 25 kHz, 25 mT/μ_0 drive field and 50 nm hydrodynamic diameter, and τ' calculated from Equation 14 (dashed). The intersection point occurs at d_c', here ∼28 nm.

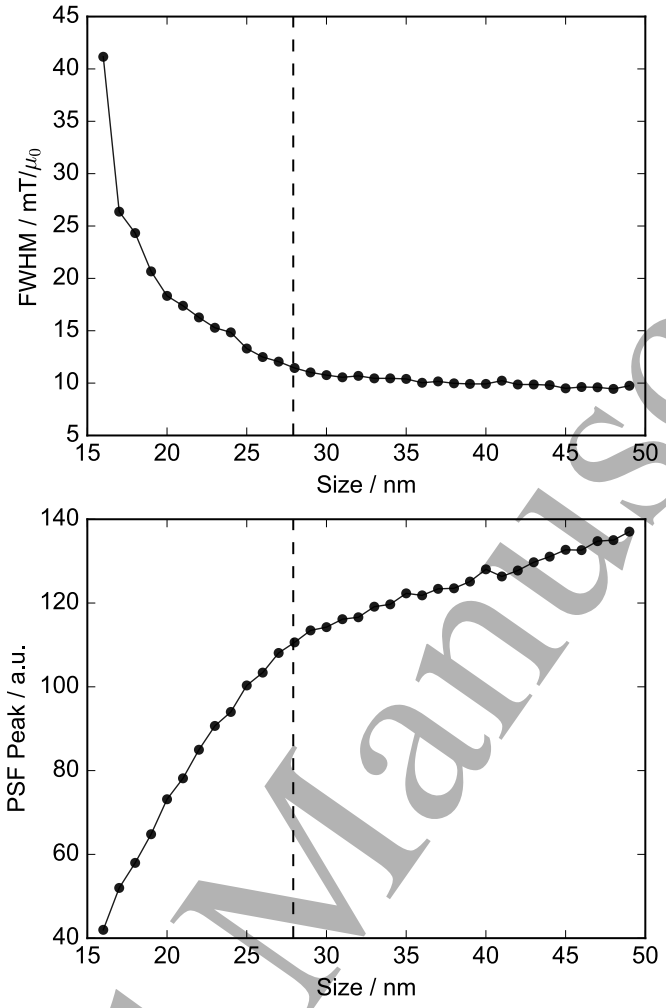

Figure 6: FWHM (top) and peak height (bottom) extracted from stochastic simulations with a 25 kHz, 25 mT/μ_0 drive field and 50 nm hydrodynamic diameter. d_c' is indicated by the dashed line in both.

Fig. 6 shows the size-dependent FWHM and PSF peak as a function of core size, with d_c' indicated. It is clear that d_c' occurs near a critical change in the slope in each case, indicating a shift in the size-dependent behavior. For $d_c < d_c'$, the rate of change of the FWHM (Δx) and the PSF peak as a function of size is noticeably greater than when $d_c > d_c'$. Increasing the core size past d_c', then, will result in minimal improvements to the MPI image quality.

Due to practical difficulties in fabricating large monodisperse particles, as well as increased likelihood for particle agglomeration, resulting in a decrease in signal quality, with large particles (which will be discussed in the following subsection), identifying this critical size d_c' is desirable. Since the particle relaxation behavior is sensitive to many internal and external properties, d_c' will also be dependent on factors such as the applied field amplitude, applied field frequency, and non-magnetic coating size. d_c' for a few common field conditions is shown in Table 1.

For typical drive field conditions used for MPI, d_c' lies between 27-29 nm. d_c' generally decreases with increasing field strength, implying that particles with sizes on the low end of that range would result in a better MPI signal when the field amplitude is stronger, i.e. when relaxation effects become more prominent. d_c' also generally decreases with increasing field frequency, again implying that smaller particles (closer to 27 nm) would result in better MPI image quality for high-frequency fields, again due to the larger relaxation effects that arise when MNPs are subjected to high-frequency fields.

Assuming that the particles are able to freely rotate, which should be the case when they are dispersed in an aqueous solution, as is typical for MPI applications, the hydrodynamic size of the MNPs will affect the relaxation

Table 1: d_c', in nanometers, for different applied field conditions, assuming a hydrodynamic diameter of 50 nm, and incorporating uncertainty from the polydispersity of typical nanoparticle size distributions.

	15 mT/μ_0	20 mT/μ_0	30 mT/μ_0
5 kHz	28.5 ± 0.1	28.2 ± 0.1	27.7 ± 0.1
10 kHz	28.9 ± 0.2	28.6 ± 0.1	28.3 ± 0.1
25 kHz	28.0 ± 0.3	28.0 ± 0.2	27.9 ± 0.1

dynamics as well, as was seen in Figure 4. In addition to the magnetic core, a non-magnetic coating such as polyethylene-glycol (PEG) must be applied to the MNP surface to allow for the dispersal of the particles in water and enable functionalization for specific clinical applications. Adding larger surface coatings increases the bulk inertia of the MNPs and so inhibits the physical rotation of the nanoparticle, typically resulting in increased relaxation time particularly for large (>20 nm) core sizes.

5 Dipolar interactions

According to the results in Fig. 2, for small hydrodynamic sizes, increasing the core size should continue to incrementally improve the MPI signal quality, at least up to core diameters of ∼40 nm, despite the onset of the dominance of relaxation effects at ∼28 nm. However, from a practical standpoint, when particle core size is further increased past ∼28 nm, particles begin to agglomerate in solution due to increased dipole-dipole interaction strength, causing significant difficulties in the phase-transfer process as well as resulting in decreased signal quality. We assume that the MNPs used as MPI tracers are single-domain and superparamagnetic, and so can be individually described as a single magnetic dipole with magnetic moment magnitude $\mu = M_s V_c$. The interaction energy between two magnetic dipoles is:

$$U_{\text{int}} = -\frac{\mu_1 \mu_2 \mu_0}{4\pi r^3} \left(3(\mathbf{m_1} \cdot \hat{\mathbf{r}})(\mathbf{m}_2 \cdot \hat{\mathbf{r}}) - \mathbf{m_1} \cdot \mathbf{m_2}\right), \tag{15}$$

where $\mathbf{r}$ is a vector pointing from the location of the first dipole to the second. If we assume that the minimum distance r that two particles can be separated by is equal to their hydrodynamic diameters, we can calculate the maximum dipole interaction energy per particle for a collection of monosized particles, and compare that value to the thermal energy $k_B T$. If the maximum interaction energy is larger than $k_B T$, then there is a significant likelihood that the particles may agglomerate in solution, or otherwise interact in a way that will cause a reduction in signal. Here, we use only this simplistic model of particle agglomeration for our calculations; however, it should be noted that more advanced modeling techniques have been used to study particle agglomeration and interparticle interactions in the past, e.g. Ref. [26], and in particular, our work in Ref. [27] which utilized the same stochastic simulations described here. In that latter work, it was found that the simple method of comparing the thermal interaction energy to the maximum interaction energy was sufficient as a first approximation for predicting the reduction of MPS signal due to interparticle interactions, and generally agreed with the more advanced stochastic simulation results. It should be acknowledged, though, that this approximation is limited in that it does not incorporate the effects of an external applied field on particle agglomeration, or other biologically or chemically relevant causes for agglomeration.

The maximum interaction energy as a function of MNP core size is shown in Fig. 7 (top). For a given hydrodynamic diameter, the maximum core size for which the interaction energy is less than the thermal energy can be extracted (assuming that the particles are held at room temperature). We will label this size d_c^*. d_c^* as a function of coating size is shown in Fig. 7 (bottom). From there we can see that for particles 27-29 nm in core diameter, the coating would need to be a minimum of 80 nm to fully prevent agglomeration.

Common coatings for MNPs used for MPI are 5 kDa, 10 kDa, and 20 kDa PEG, which typically result in hydrodynamic sizes of between 40 nm and 150 nm for 20-25 nm core sizes. For particles with a core size of 30 nm or greater, the coating would need to be a minimum of 100 nm to prevent agglomeration, and so would preclude the use of 5 kDa and possibly 10 kDa PEG. Furthermore, difficulties during the coating process itself often arise when particle cores are larger than ∼30 nm due to interparticle interactions.

In Table 2, the smaller of d_c' and d_c^* is shown for three different hydrodynamic diameters, which represent the common range for MNPs functionalized for long-term circulation with MPI, indicating the optimal core size that should be used for minimizing both relaxation and interaction effects, while maximizing performance. When the hydrodynamic size is at least 100 nm, d_c' is typically smaller, whereas when the hydrodynamic size is decreased

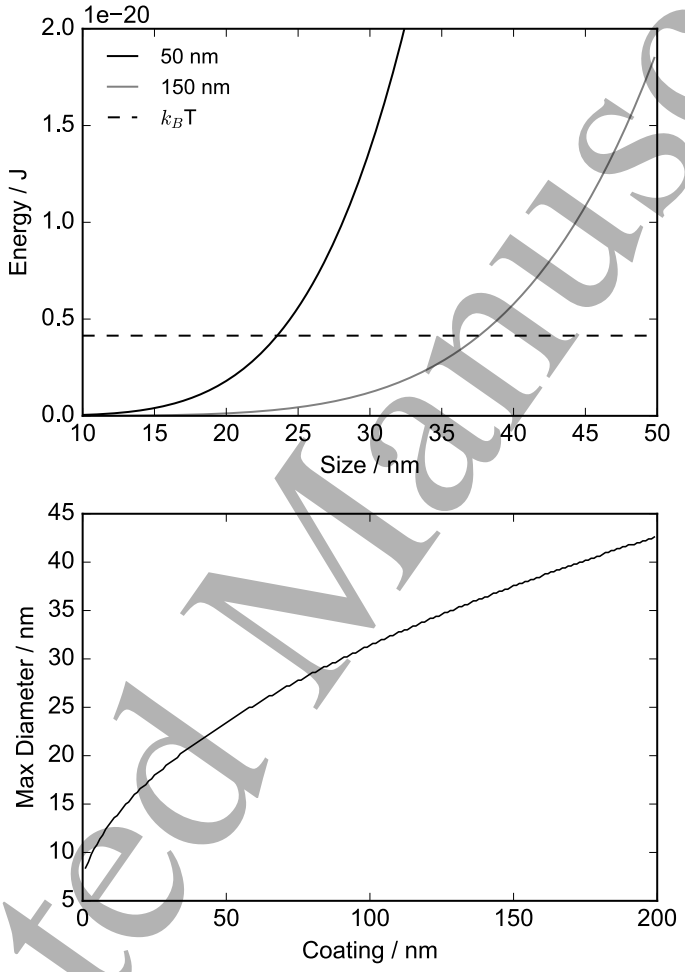

Figure 7: Top: Maximum interaction energy vs. core size for two different hydrodynamic sizes. Thermal energy is indicated by the dashed line. Bottom: The maximum particle diameter (d_c^*) at which the maximum interaction energy is lower than the thermal energy, as a function of coating size.

Table 2: The smaller of d_c' and d_c^* for common MPI field conditions and three different hydrodynamic diameters (representing different sizes of tracer coatings), incorporating uncertainty from the polydispersity of typical nanoparticle size distributions.

50 nm			
	15 mT/μ_0	20 mT/μ_0	30 mT/μ_0
5 kHz	23.1 ± 0.1	23.1 ± 0.1	23.1 ± 0.1
10 kHz	23.1 ± 0.2	23.1 ± 0.1	23.1 ± 0.1
25 kHz	23.1 ± 0.3	23.1 ± 0.2	23.1 ± 0.1

100 nm			
	15 mT/μ_0	20 mT/μ_0	30 mT/μ_0
5 kHz	29.6 ± 0.1	29.4 ± 0.1	29.1 ± 0.1
10 kHz	29.1 ± 0.2	29.1 ± 0.1	29.1 ± 0.1
25 kHz	27.7 ± 0.3	27.7 ± 0.2	27.6 ± 0.1

150 nm			
	15 mT/μ_0	20 mT/μ_0	30 mT/μ_0
5 kHz	29.4 ± 0.1	29.5 ± 0.1	29.4 ± 0.1
10 kHz	28.6 ± 0.2	28.6 ± 0.1	28.6 ± 0.1
25 kHz	27.4 ± 0.3	27.3 ± 0.2	27.1 ± 0.1

Table 3: The smaller of d_c' and d_c^* for particles with a 100 nm coating under a 25 kHz, 20 mT/μ_0 field, for different values of the anisotropy constant, incorporating uncertainty from the polydispersity of typical nanoparticle size distributions.

K	5 kJ/m^3	7 kJ/m^3	9 kJ/m^3	11 kJ/m^3
d_c	27.7 ± 0.2	26.3 ± 0.2	24.4 ± 0.3	23.1 ± 0.3

to below 100 nm, dipole interactions start to significantly limit the maximum core size that should be used. This indicates that when small coatings (e.g. 5 kDa PEG) are required, the core size should be appropriately reduced as well, otherwise increased potential for agglomeration can result in problems during the phase transfer, dispersion, or clinical application process.

Finally, we examine the effect of the anisotropy constant on the optimal core size. Identical analysis was performed for different values of K, with the results shown in Table 3. As expected, the optimal core size decreases for higher values of K due to increased relaxation effects.

6 Conclusion

In this work, the effects of size-dependent nanoparticle relaxation and interaction behavior were studied. We found that for single-core, spherical, monodisperse, magnetite nanoparticles, for typical MPI field conditions and tracer properties, increasing the core size to ∼28 nm will result in significant improvements to the predicted resulting MPI image. However, when core size is increased beyond ∼28 nm, relaxation effects dominate and improvements to the MPI signal are minimal. Furthermore, increasing the core size beyond ∼28 nm increases the potential for particle agglomeration and further decrease in signal quality. When fabricating or selecting MNP tracers to be used for MPI, then, the desired core size for single-core, magnetite nanoparticles should be around 28 nm, and then tuned based on the specifics of the hardware (e.g. applied field amplitude and frequency to be used), the surface coating, and the particle anisotropy.

Acknowledgments

CS was supported by a National Science Foundation Graduate Research Fellowship under Grant DGE-1256082. This work was facilitated through the use of advanced computational, storage, and networking infrastructure provided by the Hyak supercomputer system and funded by the STF at the University of Washington.

References

[1] Bernhard Gleich and Jürgen Weizenecker. Tomographic imaging using the nonlinear response of magnetic particles. *Nature*, 435(7046):1214, 2005.

[2] PW Goodwill, A Tamrazian, LR Croft, CD Lu, EM Johnson, R Pidaparthi, RM Ferguson, AP Khandhar, KM Krishnan, and SM Conolly. Ferrohydrodynamic relaxometry for magnetic particle imaging. *Applied Physics Letters*, 98(26):262502, 2011.

[3] Hamed Arami, RM Ferguson, Amit P Khandhar, and Kannan M Krishnan. Size-dependent ferrohydrodynamic relaxometry of magnetic particle imaging tracers in different environments. *Medical physics*, 40(7), 2013.

[4] Scott J Kemp, R Matthew Ferguson, Amit P Khandhar, and Kannan M Krishnan. Monodisperse magnetite nanoparticles with nearly ideal saturation magnetization. *RSC Advances*, 6(81):77452–77464, 2016.

[5] R Matthew Ferguson, Amit P Khandhar, and Kannan M Krishnan. Tracer design for magnetic particle imaging. *Journal of applied physics*, 111(7):07B318, 2012.

[6] Sabina Ziemian, Norbert Löwa, Olaf Kosch, Daniel Bajj, Frank Wiekhorst, and Gunnar Schütz. Optimization of iron oxide tracer synthesis for magnetic particle imaging. *Nanomaterials*, 8(4):180, 2018.

[7] Harald Kratz, Matthias Taupitz, Angela Ariza de Schellenberger, Olaf Kosch, Dietmar Eberbeck, Susanne Wagner, Lutz Trahms, Bernd Hamm, and Jörg Schnorr. Novel magnetic multicore nanoparticles designed for mpi and other biomedical applications: From synthesis to first in vivo studies. *PloS one*, 13(1):e0190214, 2018.

[8] Laura R Croft, Patrick W Goodwill, Justin J Konkle, Hamed Arami, Daniel A Price, Ada X Li, Emine U Saritas, and Steven M Conolly. Low drive field amplitude for improved image resolution in magnetic particle imaging. *Medical physics*, 43(1):424–435, 2016.

[9] Richard Mathew Ferguson, Amit P Khandhar, Hamed Arami, Loc Hua, Ondrej Hovorka, and Kannan M Krishnan. Tailoring the magnetic and pharmacokinetic properties of iron oxide magnetic particle imaging tracers. *Biomedizinische Technik/Biomedical Engineering*, 58(6):493–507, 2013.

[10] Ryan Hufschmid, Joachim Landers, Carolyn Shasha, Soma Salamon, Heiko Wende, and Kannan M Krishnan. Nanoscale physical and chemical structure of iron oxide nanoparticles for magnetic particle imaging. *physica status solidi (a)*, 216(2):1800544, 2019.

[11] R Matthew Ferguson, Kevin R Minard, and Kannan M Krishnan. Optimization of nanoparticle core size for magnetic particle imaging. *Journal of magnetism and magnetic materials*, 321(10):1548–1551, 2009.

[12] Juergen Weizenecker, Bernhard Gleich, Juergen Rahmer, and Joern Borgert. Micro-magnetic simulation study on the magnetic particle imaging performance of anisotropic mono-domain particles. *Physics in Medicine & Biology*, 57(22):7317, 2012.

[13] D Eberbeck, F Wiekhorst, S Wagner, and L Trahms. How the size distribution of magnetic nanoparticles determines their magnetic particle imaging performance. *Applied physics letters*, 98(18):182502, 2011.

[14] S Biederer, T Knopp, TF Sattel, K Lüdtke-Buzug, B Gleich, J Weizenecker, J Borgert, and TM Buzug. Magnetization response spectroscopy of superparamagnetic nanoparticles for magnetic particle imaging. *Journal of Physics D: Applied Physics*, 42(20):205007, 2009.

[15] R Matthew Ferguson, Kevin R Minard, Amit P Khandhar, and Kannan M Krishnan. Optimizing magnetite nanoparticles for mass sensitivity in magnetic particle imaging. *Medical physics*, 38(3):1619–1626, 2011.

[16] Frank Ludwig, Thilo Wawrzik, Takashi Yoshida, Nicole Gehrke, Andreas Briel, Dietmar Eberbeck, and Meinhard Schilling. Optimization of magnetic nanoparticles for magnetic particle imaging. *IEEE Transactions on Magnetics*, 48(11):3780–3783, 2012.

[17] Rohan Dhavalikar and Carlos Rinaldi. On the effect of finite magnetic relaxation on the magnetic particle imaging performance of magnetic nanoparticles. *Journal of Applied Physics*, 115(7):074308, 2014.

[18] J Weizenecker, J Borgert, and B Gleich. A simulation study on the resolution and sensitivity of magnetic particle imaging. *Physics in Medicine & Biology*, 52(21):6363, 2007.

[19] Yimeng Du, Pui Lai, Cheung Leung, and Philip Pong. Design of superparamagnetic nanoparticles for magnetic particle imaging (mpi). *International journal of molecular sciences*, 14(9):18682–18710, 2013.

[20] William T Coffey and Yuri P Kalmykov. Thermal fluctuations of magnetic nanoparticles: Fifty years after brown. *Journal of Applied Physics*, 112(12):121301, 2012.

[21] Jürgen Weizenecker. The fokker–planck equation for coupled brown–néel-rotation. *Physics in Medicine & Biology*, 63(3):035004, 2018.

[22] Frank Ludwig, Dietmar Eberbeck, Norbert Löwa, Uwe Steinhoff, Thilo Wawrzik, Meinhard Schilling, and Lutz Trahms. Characterization of magnetic nanoparticle systems with respect to their magnetic particle imaging performance. *Biomedizinische Technik/Biomedical Engineering*, 58(6):535–545, 2013.

[23] Jürgen Weizenecker, Bernhard Gleigh, Jürgen Rahmer, and Jörn Borgert. Particle dynamics of mono-domain particles in magnetic particle imaging. In *Magnetic Nanoparticles: Particle Science, Imaging Technology, and Clinical Applications*, pages 3–15. World Scientific, 2010.

[24] Carolyn Shasha, Eric Teeman, and Kannan M Krishnan. Harmonic simulation study of simultaneous nanoparticle size and viscosity differentiation. *IEEE Magnetics Letters*, 8:1–5, 2017.

[25] Frank Ludwig, Hilke Remmer, Christian Kuhlmann, Thilo Wawrzik, Hamed Arami, R Mathew Ferguson, and Kannan M Krishnan. Self-consistent magnetic properties of magnetite tracers optimized for magnetic particle imaging measured by ac susceptometry, magnetorelaxometry and magnetic particle spectroscopy. *Journal of magnetism and magnetic materials*, 360:169–173, 2014.

[26] Eldin Wee Chuan Lim and Ruili Feng. Agglomeration of magnetic nanoparticles. *The Journal of chemical physics*, 136(12):124109, 2012.

[27] Eric Teeman, Carolyn Shasha, James E Evans, and Kannan M Krishnan. Intracellular dynamics of superparamagnetic iron oxide nanoparticles for magnetic particle imaging. *Nanoscale*, 11(16):7771–7780, 2019.